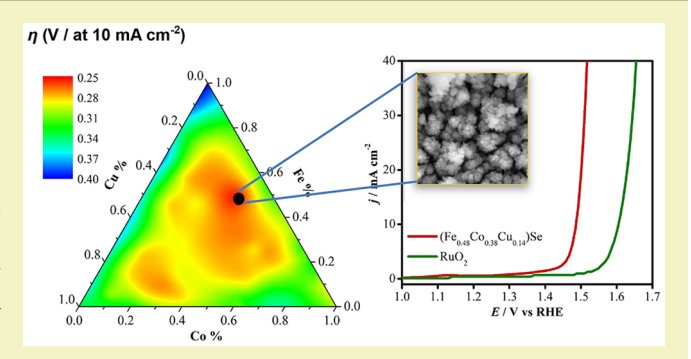


Expanding Multinary Selenide Based High-Efficiency Oxygen Evolution Electrocatalysts through Combinatorial Electrodeposition: Case Study with Fe-Cu-Co Selenides

Xi Cao, [†] Emily Johnson, [‡] and Manashi Nath*, [†]

Supporting Information

ABSTRACT: Developing low-cost electrocatalysts with high efficiency for water splitting is a critical task to make this technology viable for large-scale clean energy generation. Transition metal selenides, comprising earth abundant elements, such as Fe, Co and Cu, have gained attention as superior electrocatalysts for oxygen evolution reaction (OER) in the alkaline medium. In this article, we have systematically investigated the evolution of OER catalytic activity as a function of composition for a series of Fe-Co-Cu quaternary selenides by exploring a trigonal phase diagram. The OER activity was dependent on the quantity of Cu and Fe in the Fe-Cu-Co-Se quaternary selenide electrocatalysts, while



surprisingly, Fe-Cu ternary selenides exhibit reduced OER activity in comparison to their pure parent compounds FeSe and Cu₃Se₂. Quaternary selenides exhibited more efficient catalytic activity with increasing amount of Fe or Cu in the catalysts, and the quaternary mixed metal selenide thin film of composition (Fe_{0.48}Co_{0.38}Cu_{0.14})Se showed the best catalytic performance with a small overpotential of 256 mV at 10 mA cm⁻² and a low Tafel slope of 40.8 mV dec⁻¹ in N₂-saturated 1.0 M KOH solution. The outstanding catalytic performance of quaternary selenides may be explained by the possible electron cloud delocalization among the transition metal sites in the catalytic system through d-bands, leading to lower charge transport resistance at the catalyst-electrolyte interface as well better film conductivity, as has also been observed through electrochemical impedance spectroscopy. Such enhanced charge transfers eventually facilitate the rate of O2 release from the catalyst surface, leading to enhanced activity.

KEYWORDS: mixed metal selenides, oxygen evolution electrocatalyst, water splitting, electrocatalyst

INTRODUCTION

Hydrogen has been widely considered as an ideal alternative for sustainable energy to diminish the utilization of fossil fuels, especially in recent times when fossil fuel depletion has reached an all-time high along with the environmental pollution caused by carbon dioxide, a byproduct of fossil fuel combustion.¹⁻³ While hydrogen fuel holds tremendous promise as a clean source of energy, the production of pure hydrogen is a challenge that must be met before hydrogen fuel can replace the mature conventional technologies. Alkaline water electrolysis is a well-established technology to produce high-purity hydrogen in copious quantities for use in fuel cells and other energy storage devices.^{4,5} Water splitting includes two critical half-cell reactions: hydrogen evolution reaction (HER) at the cathode $(2H_2O + 2e^- \rightarrow H_2 + 2OH^-)$ and oxygen evolution reaction (OER) at the anode $(4OH^- \rightarrow O_2 +$ 4e⁻ + 2H₂O).⁶⁻⁹ Among these, OER is the more challenging kinetically sluggish process with multistep four-electron transfers involved which has greatly reduced the efficiency of water splitting reaction, thereby limiting the applicability of this technology to produce hydrogen on a large scale. An efficient electrocatalyst is required to speed up OER by lowering the activation barrier and reducing the overpotential required for water oxidation. In this context, a large number of research endeavors have been devoted to designing high-efficiency and low-cost OER electrocatalysts. 10-14 Although research over the last several decades has identified some stateof-the-art OER electrocatalysts based on noble metal based oxides, such as IrO2 and RuO2 exhibiting low overpotentials and excellent stability, the scarcity and high cost of these precious metals have hindered their large scale industrial applications. 15,16 Consequently, over the past several years, researchers have focused on exploring earth abundant transition metal based chemistry to identify and develop low-

Received: February 24, 2019 April 19, 2019 Revised: Published: April 23, 2019



Department of Chemistry, Missouri University of Science & Technology, 400 W. 11th Street, Rolla, Missouri 65409, United States Department of Chemical and Biochemical Engineering, Missouri University of Science & Technology, 1101 N. State Street, Rolla, Missouri 65409, United States

cost electrocatalysts comprising first row transition metals (primarily Fe, Ni, and Co). The quest for these transition metal electrocatalysts has led to oxides and (oxy)hydroxides, which could potentially replace precious metals due to their comparable activity and durability. 17-24 Continued research conducted by our group as well as by other groups over the last couple of years has made it quite apparent that transition metal based selenides are more likely to exhibit an improved OER catalytic activity and a reduced overpotential compared to oxides. Such enhancement of OER catalytic activity is attributed to the increased covalency of the metal-ligand bond as well as lowering the electrochemical redox potential of the catalytically active transition metal site. 25-30 It was also observed that the smaller electronegativity of selenium compared to oxygen led to the enhancement of preferential attachment of hydroxyl ions on the catalytically active metal sites and facilitated further steps of the OER process. 31-33 Accordingly, binary metal selenides (Ni₃Se₂, NiSe₂, CoSe, and Co₇Se₈) have been widely investigated as excellent OER electrocatalysts with impressively low overpotentials.^{26,34–36} Ternary mixed metal selenides such as Ni_xFe_{1-x}Se₂, Ni_{0.89}Co_{0.11}Se₂, FeNi₂Se₄, and NiCoSe₂ exhibit more efficient catalytic activity, suggesting that introduction of transition metal dopants improves catalytic activity.^{37–40} Further studies revealed that transition metal doping increased the number of actual catalytically active sites and accelerated the ratedetermining steps by modulating the OH⁻ adsorption kinetics on the catalyst surface through tuning the local electron density around the catalytic site. 41,42 Similar effects can also be observed in the transition metal oxides/(oxy)hydroxides, such as Fe or Co doped NiO/NiOOH exhibiting a much higher catalytic activity than NiO/NiOOH itself.^{43–46} More recently, we have systematically studied how transition metal doping in catalytically active selenide compositions affect OER activity through the exploration of a trigonal phase diagram of Ni-Fe-Co selenides and demonstrated that quaternary mixed metal selenides exhibited better OER activity than binary or even ternary selenides.³³ In the Ni-Fe-Co selenide system, quaternary selenides with a progressively increasing amount of Fe showed higher catalytic activity and the optimal composition was identified as (Ni_{0.25}Fe_{0.68}Co_{0.07})₃Se₄ which could achieve 10 mA cm⁻² at a small overpotential of 230 mV and showed remarkable durability in alkaline medium.³³ While Ni and Co have traditionally shown excellent OER activity and have been given primary attention due to their relative abundance on the earth's crust compared to precious metals, another abundant element with high d-electron occupancy, namely copper, has been explored far less for electrocatalytic water splitting. Cu based OER electrocatalysts will be even more impactful since copper is one of the most abundant elements on the earth's crust found in lots of minerals.⁴⁷ Very recently, there has been a couple of reports where Cu₂O has been reported as an OER active catalyst. 48,49 We have synthesized Cu₂Se via electrodeposition as well as hydrothermal and high temperature chemical vapor deposition methods and have shown that Cu₂Se exhibited better electrocatalytic activity compared to the oxide analogue.⁵ Additionally, introduction of Cu with highly occupied *d*-levels imparts enhanced conductivity to the matrix which will improve charge transport on the catalyst surface. Hence, to understand the effect of transition metal doping in copper selenide on the OER catalytic activity, we have performed a systemic study of the phase diagram of Co-Ni-Cu

selenides.⁵¹ These studies reveal that OER catalytic activity is influenced by the amount of Cu introduced into the catalytic system, specifically for quaternary selenides, and the bestperforming catalyst composition in this case was identified as (Co_{0.21}Ni_{0.25}Cu_{0.54})₃Se₂ thin film, which required an overpotential of 272 mV to reach 10 mA cm^{-2.51} Fe has been shown to act as an enhancer for OER catalytic activity in oxides and selenides, 33,52,53 and quaternary selenides incorporating both Cu and Fe are expected to have better OER catalytic activity. Inspired by this idea, we have systematically investigated a series of mixed metal selenides comprising various amounts of Fe, Co, and Cu by exploring a trigonal phase diagram through combinatorial electrodeposition as has been reported in this article. Surprisingly, Fe-Cu ternary selenides showed reduced OER activity in comparison to their pure parent compounds FeSe and Cu₃Se₂, indicating that neither Fe nor Cu doping can improve the activity of Cu₃Se₂ or FeSe, respectively. On the other hand, with introduction of Co dopant into the composition, all Fe-Co-Cu quaternary selenides showed enhanced catalytic activity with low overpotential as well as lower Tafel slopes. The catalytic activity of the quaternary selenides improved as the relative amounts of either Fe or Cu increased in the catalysts. The optimal catalyst composition in this phase space was identified as (Fe_{0.48}Co_{0.38}Cu_{0.14})Se, which required an overpotential of 256 mV to achieve 10 mA cm⁻² and showed Tafel slope of 40.8 mV dec⁻¹. The low value of the Tafel slope indicates that the catalyst has favorable kinetics for OER in alkaline medium. It is interesting to note that even in the absence of Ni, which has been recognized as one of the most active catalytic sites, it is possible to have high-efficiency catalytic activity for OER through transition metal doping. The enhanced catalytic activity can be attributed to the possible electron cloud delocalization through formation of d-bands between the different transition metal centers within the catalytic system.^{7,54} This systematic exploration of mixed metal selenides composed of iron, cobalt, and copper offers more opportunities to understand the evolution of the catalytic property as a function of covalency and *d*-electron occupancy of the transition metals and will have far-reaching implications in practical application of electrocatalytic water splitting.

■ EXPERIMENTAL SECTION

Materials. The metal precursors comprising iron(II) sulfate [FeSO₄·7H₂O, 99.0%], cobalt(II) sulfate [CoSO₄·7H₂O, 99.0%], copper(II) sulfate [CuSO₄·5H₂O, 99.0%], selenium dioxide [SeO₂], ammonium sulfate [(NH₄)₂SO₄, 99%], and potassium hydroxide [KOH, 85.0%] were obtained from Fisher Scientific and used as received. All solutions were prepared in deionized (DI) water (18 MΩ/cm). The Au-coated glass substrates used in electrodeposition were purchased from Deposition Research Lab Incorporated (DRLI), Lebanon, Missouri.

Combinatorial Electrodeposition of Thin Films. Systematic exploration of a trigonal phase diagram was carried out to synthesize a series of transition metal doped ternary and quaternary selenide films through combinatorial electrodeposition as shown in Figure S1. This method is very similar to our previously reported work featuring Co–Fe–Ni selenides, and the process has been described in detail in a previous publication.³³ Specifically, the electrolyte contained a combination of freshly prepared 10 mM FeSO₄·7H₂O, CoSO₄·7H₂O, and CuSO₄·5H₂O solutions along with 10 mM SeO₂ and 25 mM (NH₄)₂SO₄. Before electrodeposition, all electrolytes were purged with N₂ for 30 min to remove dissolved oxygen. Prior to electrodeposition, Au-coated glass substrates were sonicated in micro-90, isopropyl alcohol followed by rinsing with deionized water to

obtain a clean surface. 33,51 To ensure the same geometric area for all electrodeposited thin films studied in this article, the cleaned substrates were confined with Teflon tape punched with a hole of known geometric area. An IviumStat potentiostat was used for all the electrodeposition experiments. The films were deposited on Aucoated glass working electrode using a three-electrode electrochemical cell consisting of a AglAgCl (KCl saturated) reference electrode and a glassy carbon (GC) counter electrode. The electrodeposition potential was maintained at -0.8 V vs AglAgCl (KCl saturated) for 300 s at room temperature.

Characterization. A KRATOS AXIS 165 X-ray photoelectron spectrometer along with the monochromatic Al X-ray source were used to conduct X-ray photoelectron spectroscopy (XPS) of the catalyst. All XPS analysis was collected on the as-prepared sample surface without any sputtering. The morphologies of the thin film before and after electrochemical activity were observed with scanning electron microscopy (SEM) using the FEI Helios NanoLab 600 FIB/ FESEM at an accelerating voltage of 15 kV and a working distance of around 5.0 mm. Energy dispersive spectroscopy (EDS) from the same SEM microscope was used to evaluate the elemental compositions of all electrodeposited films. In this work, the elemental analysis was obtained at three to five different spots on the surface of each compound and the average EDS data was considered for obtaining the relative atomic ratio of the constituent elements. For all compounds, the molecular formula was written as $(Fe_xCo_yCu_z)Se_y$, where x, y, z, and n were the EDS atomic ratios of the transition elements to total amount of selenium, respectively.

■ ELECTROCHEMICAL MEASUREMENTS

A typical three-electrode electrochemical cell connected to an IviumStat potentiostat was used for measuring the electrocatalytic performances. Linear sweep voltammetry (LSV) was carried out to study the OER catalytic activity, while the catalyst stability was investigated by carrying out constant potential chronoamperometry for an extended period of time in N₂-saturated 1.0 M KOH at room temperature. In all the electrochemical experiments, the deposited thin films served as the working electrode, while GC was used as the counter electrode and AglAgCl (KCl saturated) as the reference electrode. The Nernst equation as shown in eq 1 was used to convert the experimentally measured potentials vs AglAgCl (KCl saturated) to the reversible hydrogen electrode (RHE).

$$E_{\text{RHE}} = E_{\text{Ag|AgCl}} + 0.059 \text{ pH} + E_{\text{Ag|AgCl}}^{\text{o}} \tag{1}$$

The standard potential of AglAgCl (KCl saturated) at 25.1 $^{\circ}$ C was 0.197 V. All the potentials reported in this article have been iR corrected.

■ CALCULATION OF TAFEL PLOT

Tafel equation relating the overpotential η with the current density j as shown in eq 2 was used to study the electrochemical kinetics of the $(Fe_xCo_yCu_z)Se_n$ thin films for OER.

$$\eta = a + \frac{2.3RT}{\alpha nF} \log(j) \tag{2}$$

Here η refers to the overpotential and j represents the current density. The Tafel slope is given by 2.3RT/an. The Tafel plots in this work were calculated from the LSV collected at a scan rate of 2 mV s⁻¹ in a nonstirred N₂-saturated 1.0 M KOH solution.

■ ELECTROCHEMICALLY ACTIVE SURFACE AREA (ECSA)

Electrochemical double layer capacitance was used to measure the ECSA of these catalysts following standard methods described in detail in previous reports. 17,33 In the measurement of ECSA through double layer capacitance, it is assumed that the current obtained in the non-Faradaic region is caused by double-layer charging instead of electrochemical reactions or charge transfer. The double layer current ($i_{\rm DL}$) was obtained by performing cyclic voltammograms (CVs) with various scan rates in a nonstirred N₂-saturated 1.0 M KOH solution. The ratio of double-layer current $i_{\rm DL}$ and the scan rate (ν) of CV yielded specific electrochemical double-layer capacitance ($C_{\rm DL}$) as shown in eq 3. The cathodic and anodic charging currents were a function of scan rates, and the $C_{\rm DL}$ can be calculated by averaging the absolute values of cathodic and anodic slopes. Equation 4 can be used to calculate ECSA.

$$i_{\rm DL} = C_{\rm DL} \times \nu \tag{3}$$

$$ECSA = C_{DL}/C_{s}$$
 (4)

Here, double-layer capacitance ($C_{\rm DL}$) is in units of mF. Based on other reported values, the specific capacitance ($C_{\rm s}$) was assumed to be 0.040 mF cm⁻² in the alkaline solution. ^{17,26} Roughness factor (RF) was estimated from the ratio of ECSA and the geometric area (0.07 cm²).

RESULTS AND DISCUSSION

Structural and Elemental Compositions of Electrodeposited Thin Films. The trigonal phase diagram as shown in Figure S1 was systematically explored to electrodeposit a series of mixed metal selenides. This method, referred to as combinatorial electrodeposition, is similar to our previous published reports where the process has been described in detail with different transition metals. 33,51 In the trigonal phase diagram, the vertices represented three binary selenides (CoSe, FeSe, and Cu₃Se₂), while the sides of the triangle referred to the ternary selenides Fe_xCo_ySe_n, Fe_xCu_ySe_n, and Co_xCu_ySe_n, respectively. The interior of this trigonal phase diagram represented the quaternary mixed metal selenides (Fe_xCo_yCu_zSe_n). It should be noted here that all the electrodeposited thin films of ternary and quaternary compositions were amorphous in nature and did not yield clear powder X-ray diffraction (PXRD) patterns, making proper phase determination from PXRD alone less probable. The elemental composition of the electrodeposited films, on the other hand, were determined from the average relative atomic ratio obtained from EDS analysis as listed in Table S1, juxtaposed with the precursor ratio in the electrolyte that produced the respective film. Typically, EDS was collected at several regions on the sample surface and, interestingly, it showed similar quantification results for the elemental ratio, indicating that while the films were not crystalline, they were indeed of uniform composition throughout each catalytic surface. As can be seen in Table S1, three as-prepared binary thin films were composed of Fe, Co or Cu and Se with approximate atomic ratios of 1:1 (Fe: Se), 1:1 (Co: Se), and 3:2 (Cu: Se) respectively, hence the molecular formula of three binaries were written as FeSe, CoSe, and Cu₃Se₂ as shown in Table S2, respectively. The molecular formulae identified in the various current voltage plots of the ternary and quaternary selenides can be found in Table S2. Careful observation of Table S1 revealed that increasing (or decreasing) amounts of

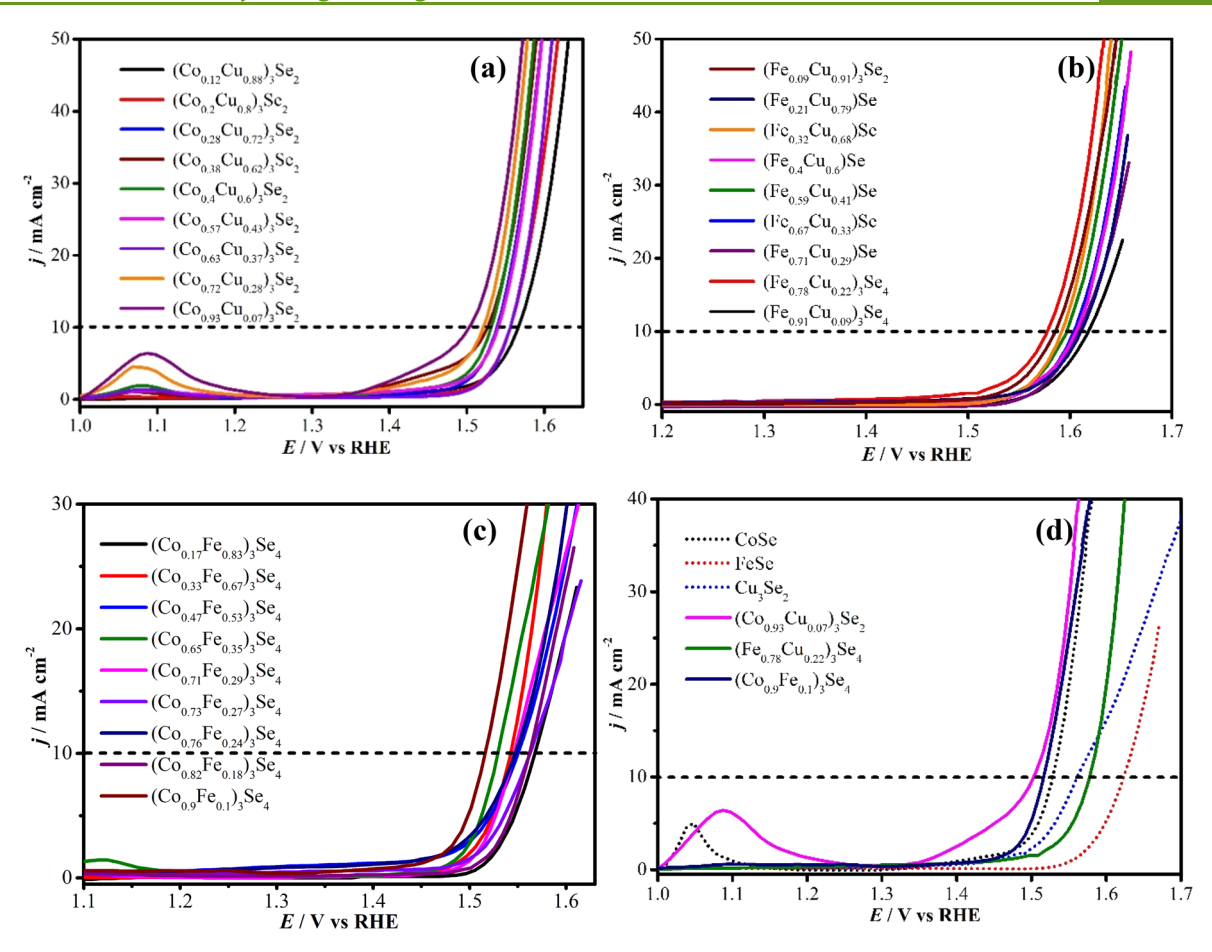


Figure 1. OER electrocatalytic performances of the various ternary metal selenides obtained along the edges of the trigonal phase diagram measured through linear sweep voltammetries (LSVs). (a) Co–Cu group, (b) Fe–Cu group, and (c) Co–Fe group. (d) OER activity of the most active ternary composition (solid line) from each group was compared with the three binary compositions (dotted line). The dashed black line in each panel indicates the current density at 10 mA cm⁻².

the metal precursor in the electrolytic bath led to an increase (or decrease) of the relative atomic percentage of the corresponding element in the electrodeposited film. This demonstrates the ability to control thin film composition through combinatorial electrodeposition.

Electrochemical Characterization. Linear sweep voltammetry (LSV) was carried out in N2-saturated 1.0 M KOH at a scan rate of 10 mV s⁻¹ to measure OER catalytic activity of the deposited films. The electrocatalytic performance was benchmarked in comparison with other highly active catalysts by comparing the onset overpotential (onset η) and the overpotential required to reach a current density of 10 mA cm⁻² (η at 10 mÅ cm⁻²) obtained from the LSV data.¹⁷ Table S1 lists the onset overpotential, overpotential at 10 mA cm⁻², and the corresponding EDS atomic ratios of all the electrodeposited selenides reported in this work. The OER polarization curves of the three binary selenide films can be found in Figure S2, demonstrating the OER catalytic activity trend of binary films was CoSe > Cu₃Se₂ > FeSe. The LSV plots for all the ternary selenide films are shown in Figure 1. In Figure 1a, Co-Cu selenides were obviously the best group in comparison to the other two, and the optimal composition in this group was identified as $(Co_{0.93}Cu_{0.07})_3Se_2$ where onset overpotential was 235 mV and overpotential was 272 mV at 10 mA cm⁻². Interestingly, the LSV plots of the Fe-Cu selenide group in Figure 1b displayed the worst catalytic activity among the three ternary groups. The ternary composition in this group that exhibited the best catalytic activity with an onset overpotential of 307 mV and an overpotential of 347 mV to reach a current density of 10 mA cm⁻² was identified as(Fe_{0.78}Cu_{0.22})₃Se₄. Some of the LSV plots from the Co-Fe selenide group shown in Figure 1c were also included in our previous work on combinatorial electrodeposition of Ni-Co-Fe multinary selenides.³³ In this group, $(Co_{0.90}Fe_{0.10})_3Se_4$ exhibited the lowest onset overpotential of 257 mV and overpotential of 295 mV at 10 mA cm^{-2,33} It is worth mentioning that several preoxidation peaks were observed in these LSVs prior to the OER process corresponding to oxidation of transition metal ions within the catalyst composite as shown in Figure 1a,d. Preoxidation peaks are commonly observed in the Ni- and Co based electrocatalysts, which result from the change in oxidation state of transition metal during the anodic scan. 55-58 As can be seen in Figure 1a,d, the peaks observed around 1.10 V vs RHE were attributed to the conversion of $\mathrm{Co^{2+}}$ to $\mathrm{Co^{3+.33,57,59}}$ Interestingly, the intensity of Co preoxidation peaks increased with increasing the amount of Co in the electrocatalysts, which further confirmed combinatorial electrodeposition as a feasible method for compositional control. The polarization curves of the most efficient ternary selenide composition from each group has been compared with those of the binaries in Figure 1d to illustrate the effect of transition metal doping on OER catalytic activity. It was observed that doping CoSe with 7% Cu improved the OER catalytic activity by decreasing η at 10 mA

ACS Sustainable Chemistry & Engineering

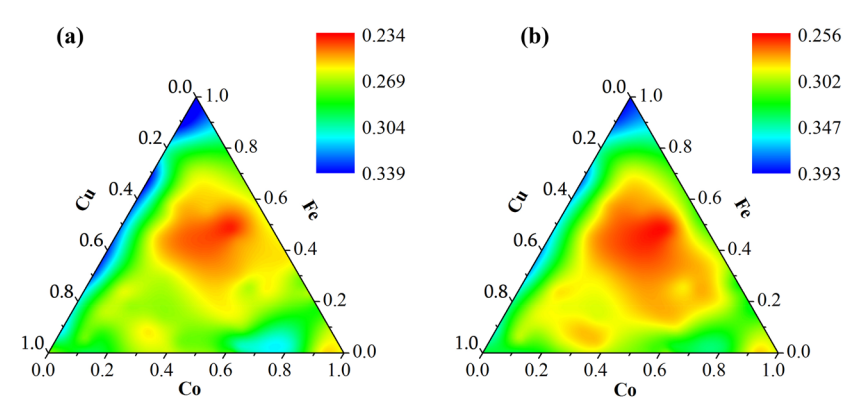


Figure 2. Trend of OER catalytic activity within the entire Fe–Co–Cu trigonal phase space. Mapping of overpotential η (in units of V) (a) at the onset of OER activity and (b) at a current density of 10 mA cm⁻². These contour plots were created by using the actual relative atomic ratio of the elements as obtained from EDS. The color gradient represents the overpotential measured in volts.

cm⁻² by about 26 mV. Similarly, 22% Cu dopant in FeSe lowered the overpotential by 46 mV to reach a current density of 10 mA cm⁻². However, it should be noted that the catalytic activity of (Fe_{0.78}Cu_{0.22})₃Se₄ was still observed to be worse than the binary copper selenide, Cu₃Se₂. Doping of of 10% Fe into CoSe did not lead to any observable change in the OER catalytic activity. It has been widely reported that incorporation of transition metal dopants improved the OER catalytic activity: for example, a small amount of Fe doped into Ni- or Co based electrocatalysts can radically ameliorate the OER activity. 43,60-66 It is interesting to note that in these ternary metal selenides, transition metal doping forces the formation of a different stoichiometry and structure type compared to the binary selenide. The ternary films of Co-Cu selenides formed the M_3Se_2 composition, and accordingly they could be described as Co-doped Cu₃Se₂. On the other hand, the Co-Fe selenide group formed the structure type M₃Se₄ Interestingly, the Fe-Cu group exhibits different stoichiometries at different relative ratios of Fe and Cu. At high Cu concentration with minimal Fe doping, the deposition adopts M₃Se₂ composition and can be described as doped Fe-doped Cu₃Se₂. At a high relative ratio of Fe with minimal Cu doping, the structure can be described as M_3Se_4 (Cu-doped Fe₃Se₄). At comparable relative ratios of Fe:Cu, the stoichiometries obtained were closer to monoselenides, and can be described as MSe. It should also be noted that each of these stoichiometries are distinctly different from each other with respect to crystal structure and may also contain different coordination geometry around the transition metal ions, as discussed later. Different stoichiometries of the metal selenides also give rise to different catalytic properties, as has been observed with the Ni-selenide, Ni₃Se₂, NiSe, NiSe₂, and Ni₃Se₄. ^{26,27,67,68} Additionally, for mixed metal catalysts, it has been shown that the OER activity depends not only on the quantity of transition metal dopants but also is strongly related to the location of metal dopants in the catalytic system. D. Friebel et al. have reported that Fe in Ni_{1-x}Fe_xOOH showed a 500-fold increase in OER activity when Fe was doped into the octahedral sites where the edge-sharing of [NiO₆] and [FeO₆] occurred affecting the local electronic structure of the catalyst.⁶⁹ We have also previously reported through density functional theory (DFT) calculations that introducing dopants into the surface layers altered the adsorption energy of hydroxyl ions on the active metal sites, thereby lowering the potential to initiate OER and leading to enhancement of the

catalytic activity.³³ Hence, it is not surprising to see Fe–Cu selenides showing less efficient OER catalytic activity, which can be a reflection of the inherent property of the structure type and composition.

The trend of OER catalytic activity in the family of Co-Fe-Cu-Se quaternary selenides comprising 66 individual compositions is shown in the contour plots of Figure 2, created from the two overpotential values (onset and η at 10 mA cm⁻²) shown in Table S1 and the EDS atomic ratios. Contour plots were constructed to investigate the trend of OER onset potential and overpotential at 10 mA cm⁻² as a function of composition as shown in Figure 2a,b, respectively. The range of overpotentials obtained is represented with a color gradient, with the catalytic activity becoming better from bottom to top of the gradient scale corresponding to the lower value of the overpotential. Typically, regions with red color showed better catalytic activity compared to the blue colored regions which showed the highest overpotentials. The very interior region in the trigonal phase diagram showed the lowest overpotential as shown in Figure 2a, demonstrating the best catalytic activity, while the areas adjacent to three axes exhibited less efficient catalytic activity. This demonstrated that heavily doped quaternary selenides were most likely to exhibit higher OER catalytic activity in comparison to binary or ternary selenides in this Cu–Co–Fe phase space. As can be seen, the best quaternary selenides were confined to the region where Cu was around 10-50%, Co was about 15-50%, and Fe was roughly 30-70%. The trends indicated that the quaternary selenides showed the best catalytic performance when the level of Fe was higher, suggesting that while Fe played an important role in improving the catalytic activity, it probably was not the main catalytic site, since Fe-rich ternary phases showed poor catalytic activity as can be observed in the Co-Fe group (Figure 1c). Meanwhile, the amount of Cu affected the catalytic activity as well with the OER activity being enhanced by a modest amount of Cu. It should be noted that a relatively higher amount of Fe or Cu compared to that of Co in the catalyst is more likely to produce better activity with lower overpotentials. However, as explained above, Fe-Cu-Se ternary selenide still showed poor performance, indicating that Fe and Cu sites by themselves do not have higher catalytic activity. However, the inductive effect of these ions on the neighboring Co sites increased the catalytic activity of Co, thereby lowering the overpotentials. These observations

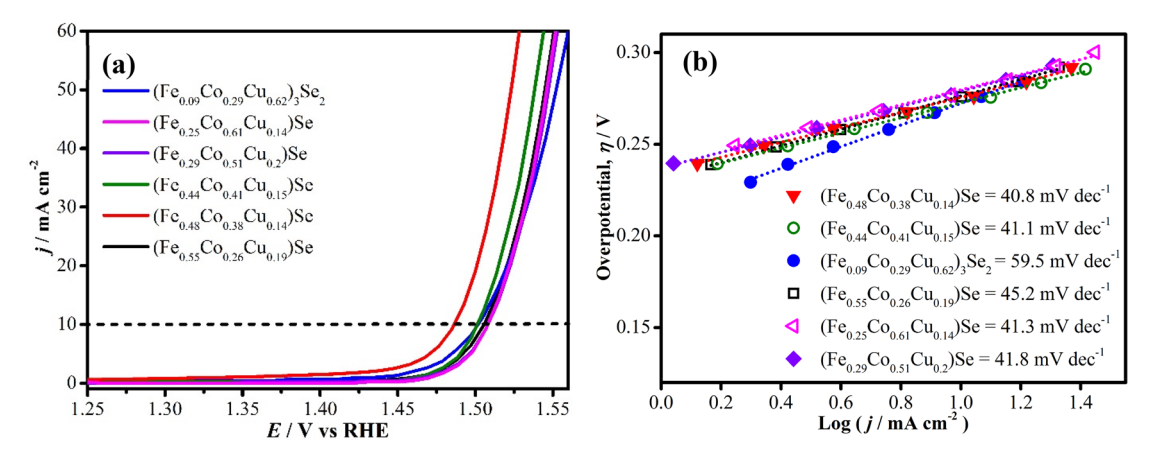


Figure 3. (a) OER activity of the six best quaternary compositions measured by conducting LSVs in N_2 -saturated 1.0 M KOH solution at a scan rate of 10 mV s⁻¹. (b) Tafel plots of these catalysts.

further confirmed the benefits of such systematic studies in discovering untargeted mixed metal based electrocatalysts.

Figure 3 indicates the LSV polarization curves of the six best performing quaternary mixed metal selenides measured in N2saturated 1.0 M KOH at scan rate of 10 mV s⁻¹. These six compounds showed excellent catalytic activity for the OER process. The onset η of $(Fe_{0.09}Co_{0.29}Cu_{0.62})_3Se_2$ was 248 mV and it needed a η of 272 mV to reach a current density of 10 mA cm⁻². The onset η and the η at 10 mA cm⁻² of (Fe_{0.25}Co_{0.61}Cu_{0.14})Se were 258 and 278 mV, respectively. The onset η of $(Fe_{0.29}Co_{0.51}Cu_{0.2})$ Se was 256 mV and it generated a current density of 10 mA cm⁻² and a η of 278 mV. The onset η of (Fe_{0.44}Co_{0.41}Cu_{0.15})Se was 250 mV and required 271 mV to achieve a current density of 10 mA cm⁻². The onset η and the η at 10 mA cm⁻² of (Fe_{0.55}Co_{0.26}Cu_{0.19})Se were 255 and 276 mV respectively. The thin film (Fe_{0.48}Co_{0.38}Cu_{0.14})Se displayed the best catalytic activity in this work, with an onset η of 235 mV and η of 256 mV at 10 mA cm⁻². It is important to note that most of the quaternary compounds adopted the monoselenide MSe structure type except for the ones with high Cu concentration, which adopted the M₃Se₂ structure type.

The Tafel slopes of all electrocatalysts were obtained, and the results are listed in Table S1. The Tafel plots (η vs log j) and slopes of the six best performing quaternary selenides are shown in Figure 3b. The Tafel slopes of (Fe_{0.55}Co_{0.26}Cu_{0.19})Se, $(Fe_{0.09}Co_{0.29}Cu_{0.62})_3Se_2$, $(Fe_{0.44}Co_{0.41}Cu_{0.15})Se$, (Fe_{0.48}Co_{0.38}Cu_{0.14})Se, (Fe_{0.29}Co_{0.51}Cu_{0.2})Se, and (Fe_{0.25}Co_{0.61}Cu_{0.14})Se were 45.2, 59.5, 41.1, 40.8, 41.8, and 41.3 mV dec⁻¹, respectively. Tafel slopes are closely related to the number of electrons involved in the rate-determining step of the OER process. For the six quaternaries with small Tafel slopes, it is likely that the second electron transfer step of OER is the rate-determining step, suggesting that they have faster kinetics for oxygen evolution. (Fe_{0.48}Co_{0.38}Cu_{0.14})Se showed the lowest overpotential as well as the lowest Tafel slope, which further confirmed that it is indeed the best catalyst composition in this quaternary phase space.

Electrochemical double-layer capacitance of the (Fe_{0.48}Co_{0.38}Cu_{0.14})Se thin film was measured to estimate its ECSA. Double-layer charging current was measured in the non-Faradaic region at various scan rates using CVs. In this study, (Fe_{0.48}Co_{0.38}Cu_{0.14})Se thin film as the working electrode was suspended in N₂-saturated 1.0 M KOH and the CVs, found in Figure 4, were measured from -0.16 to -0.05 V vs

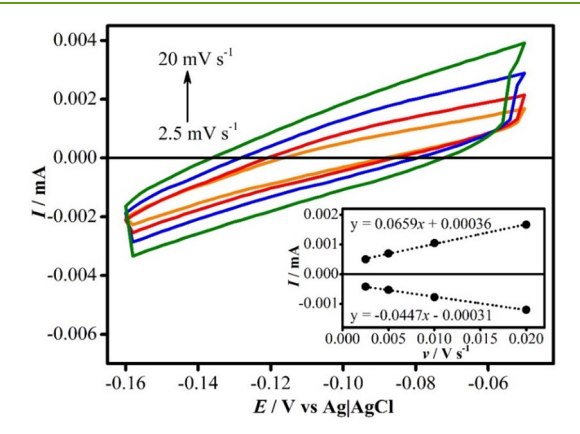


Figure 4. ECSA for the $(Fe_{0.48}Co_{0.38}Cu_{0.14})$ Se thin film was measured by performing cyclic voltammograms in N₂-saturated 1.0 M KOH solution at different scan rates from 2.5 to 20 mV s⁻¹. The inset shows the plot of both anodic and cathodic currents measured at -0.10 V vs AglAgCl (KCl saturated) as a function of scan rate.

AglAgCl (KCl saturated) at scan rates of 2.5 to 20 mV s⁻¹. The ECSA was calculated using eq 4, and the value was estimated to be 1.38 cm² with a roughness factor (RF) of 19.7. The high value of RF confirmed the highly granular surface of the film as seen in the SEM image of Figure 5b. Since rough surfaces allow for amplified contact of the electrolyte with the catalytically active sites, catalytic activity tends to increase with increasing surface roughness.

The catalytic activity of the best performing quaternary (Fe_{0.48}Co_{0.38}Cu_{0.14})Se was compared with those of CoSe, FeSe, and Cu₃Se₂ in N₂-saturated 1.0 M KOH at a scan rate of 10 mV s⁻¹ to understand the effect of transition metal doping on catalytic activity as shown in Figure 5a. The onset overpotentials of the binary selenides were 263, 346, and 270 mV for CoSe, FeSe, and Cu₃Se₂, respectively. To achieve an OER current density of 10 mA cm⁻², the overpotentials were 298, 393, and 330 mV for CoSe, FeSe, and Cu₃Se₂, respectively. As a result of transition metal doping, the onset η and η at 10 mA cm^{-2} of $(Fe_{0.48}Co_{0.38}Cu_{0.14})$ Se were decreased to 235 and 256 mV respectively, which were lower than those of any of the binary selenides. The Tafel slope of (Fe_{0.48}Co_{0.38}Cu_{0.14})Se (40.8 mV dec⁻¹) was also lower than those of CoSe (62.9 mV dec^{-1}), FeSe (103.5 mV dec^{-1}), and Cu_3Se_2 (93.4 mv dec^{-1}) as shown in Table S1, suggesting the OER activity on the quaternary selenide surface is increased kinetic factors

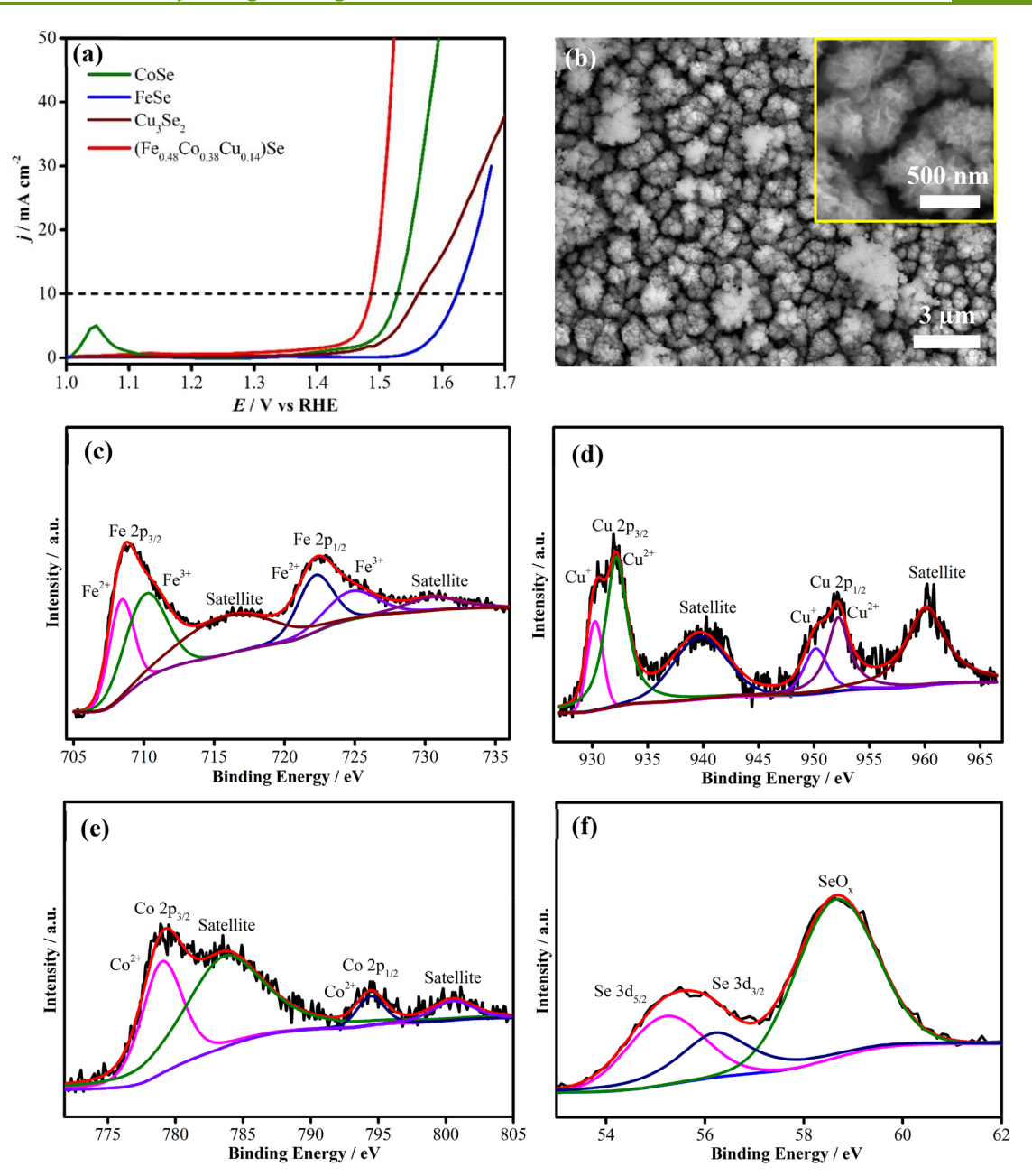


Figure 5. (a) Polarization curves of (Fe_{0.48}Co_{0.38}Cu_{0.14})Se compared with the three binary catalyst films. (b) SEM image of (Fe_{0.48}Co_{0.38}Cu_{0.14})Se film deposited for 300 s. (c-f) XPS spectra of the as-deposited (Fe_{0.48}Co_{0.38}Cu_{0.14})Se showing, (c) Fe 2p, (d) Cu 2p, (e) Co 2p, and (f) Se 3d.

compared to that on the binaries. This can be attributed to transition metal doping, which increases the amount of actual catalytically active sites as well as influence the energetics of hydroxyl attachment, thereby facilitating the OER reaction rate. The LSV curve of $(Fe_{0.48}Co_{0.38}Cu_{0.14})$ Se was also compared with the catalytic performance of the best ternary phases from each group, viz. $(Fe_{0.78}Cu_{0.22})_3Se_4$, $(Co_{0.93}Cu_{0.07})_3Se_2$, $(Co_{0.9}Fe_{0.1})_3Se_4$ shown in Figure S3. As can be seen, $(Fe_{0.48}Co_{0.38}Cu_{0.14})$ Se exhibited ameliorated OER activity compared to the best ternary composition $(Co_{0.93}Cu_{0.07})_3Se_2$ with a decrease in η at 10 mA cm $^{-2}$ by 16 mV. Overall, the OER catalytic activity was decidedly enhanced in mixed metal selenides in terms of both overpotential and Tafel slope.

The morphology and composition of the best performing quaternary selenide was further studied through surface

analytical techniques. Detailed SEM imaging of the (Fe_{0.48}Co_{0.38}Cu_{0.14})Se film as shown in Figure 5b suggested that the morphology of the thin film surface was composed primarily of cauliflower-like microstructures with a wide size distribution of 0.5 to 2.5 μ m. XPS was carried out to further study the elemental composition and identify oxidation states of the constituent elements in (Fe_{0.48}Co_{0.38}Cu_{0.14})Se thin film. The XPS spectra of Fe 2p, Cu 2p, Co 2p, and Se 3d are shown in Figure 5c-f. It should be noted that the binding energies in all XPS spectra have been calibrated with respect to the standard C 1s (284.5 eV) reference spectra. The spectrum of Fe 2p in Figure 5c showed peaks at 708.45 and 722.27 eV corresponding to Fe²⁺, while peaks at 710.26 and 724.75 eV were assigned to Fe³⁺ with satellite peaks at 716.08 and 730.57 eV.^{74–76} In the Cu 2p spectrum as shown in Figure 5d, peaks at 930.32 and 950.12 eV were attributed to Cu⁺, and those at

932.16 and 952.23 eV corresponded to Cu^{2+} respectively. Peaks at 939.75 and 960.15 eV were assigned to the satellite peaks. 77,78 In the Co 2p spectrum shown in Figure 5e, peaks at 779.14 and 794.48 eV referred to Co^{2+} , and those at 783.80 and 800.61 eV corresponded to its satellite peaks, respectively. 79,80 In the Se 3d spectrum shown in Figure 5f, peaks at 55.24 and 56.22 eV were assigned to Se $3d_{5/2}$ and Se $3d_{3/2}$ respectively, while the big sharp peak around 59.0 eV was attributed to SeO_x which might be a result of the surface oxidation of selenide. The deconvoluted spectra revealed that both Fe 2p and Cu 2p were mixed valence metal cations, while Co 2p was present as only divalent ions. The XPS spectra also confirmed that the film composition was exclusively selenide with no indication of presence of other metal oxide/oxyhydroxide impurity.

The Faradaic efficiency of the electrodeposited (Fe_{0.48}Co_{0.38}Cu_{0.14})Se thin film for OER was assessed with the water displacement method, ⁸³ and the measured quantity of O₂ evolved was compared to the theoretical yield as shown in Figure 6. A Faradaic efficiency of nearly 100% was measured for this electrocatalyst.

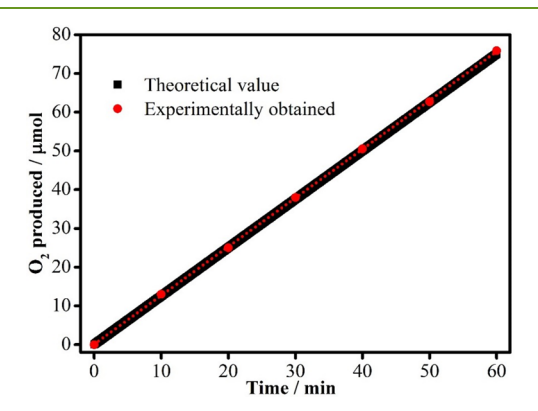


Figure 6. Amount of theoretically calculated oxygen (black dots) and experimentally measured oxygen (red dots) obtained for $(Fe_{0.48}Co_{0.38}Cu_{0.14})Se$ versus time at 0.7 V vs AglAgCl (KCl saturated).

As mentioned above, transition metal doping is expected to influence electron density through an inductive effect around the catalytic centers, and hence will influence charge transport at the catalyst-electrolyte interface as well as through the catalyst composite. Electrochemical impedance spectroscopy (EIS) was executed on the best performing quaternary composition along with the three binary selenide films to examine the result of transition metal doping on the various charge transfer pathways. Figure 7 shows the Nyquist plots of the best-performance quaternary selenide, (Fe_{0.48}Co_{0.38}Cu_{0.14})-Se, compared with those of three binary selenides (FeSe, CoSe, and Cu₃Se₂), which were collected at an applied potential of 0.5 V vs AglAgCl (KCl saturated) in N2-saturated 1.0 M KOH solution. The Nyquist plots were fitted to an equivalent circuit as shown in inset of Figure 7, which included the electrolyte resistance (R_s) , interfacial electron charge transfer resistance (R_{ct}) , and the constant phase element of double layer (CPE_{dl}). The values of these parameters are listed in Table 1. In the higher frequency region, the low value of R_s of ca. 5.0 Ω was attributed to the uncompensated solution resistance of 1.0 M KOH (Figure S4). Derived from the equivalent circuit, the charge transfer resistance (R_{ct}) and constant phase element of

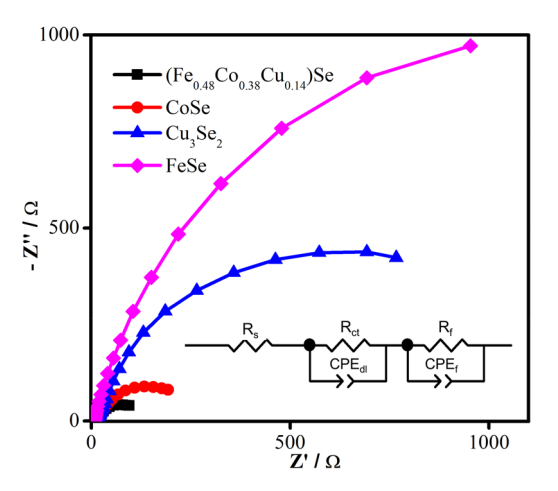


Figure 7. EIS measurements and the corresponding Nyquist plots for $(Fe_{0.48}Co_{0.38}Cu_{0.14})Se$, CoSe, Cu_3Se_2 , and FeSe catalysts obtained at an applied potential of 0.5 V vs AglAgCl (KCl saturated) in N₂-saturated 1.0 M KOH solution. Symbols indicate the raw data, while solid lines represent the corresponding fit to equivalent circuit model (inset).

Table 1. Equivalent Circuit Parameters Obtained from Fitting of EIS Experimental Data

Catalysts	$\stackrel{R_{ m s}}{(\Omega)}$	$R_{\mathrm{ct}}\left(\Omega\right)$	$ \begin{array}{c} \text{CPE}_{dl} \\ \text{(F)} \end{array} $	$R_{\mathrm{f}}\left(\Omega\right)$	$ \begin{array}{c} \text{CPE}_{\text{f}} \\ \text{(F)} \end{array} $
$(Fe_{0.48}Co_{0.38}Cu_{0.14})Se$	5.0	10.9	0.24	113.1	0.80
CoSe	5.0	13.2	0.30	248.9	0.83
Cu_3Se_2	5.0	18.4	0.48	1022.3	0.87
FeSe	5.0	291.9	0.75	2040.0	0.93

 $^aR_{\rm s}$ is the resistance of the electrolyte; $R_{\rm ct}$ is the electron transfer resistance; ${\rm CPE_{dl}}$ is the constant phase element of double-layer nonideal capacitance; $R_{\rm f}$ is resistance of the catalyst layer; and ${\rm CPE_{f}}$ is the capacitance.

double layer (CPE_{dl}) were obtained in the lower-frequency region. The charge transfer resistance R_{ct} is related to the electron transfer across the electrode-electrolyte interface and hence represents the kinetics of the electrocatalysis and its value is inversely proportional to the reaction rate. 84-86 From Table 1, it can be seen that (Fe_{0.48}Co_{0.38}Cu_{0.14})Se showed the smallest R_{ct} value, indicating that, at the film-electrolyte interface, the charge transfer rate was kinetically faster for (Fe_{0.48}Co_{0.38}Cu_{0.14})Se than those of binaries (CoSe, Cu₃Se₂, and FeSe). Fast interfacial charge transfer leads to high catalytic efficiency of (Fe_{0.48}Co_{0.38}Cu_{0.14})Se by facilitating the rate of intermediate formation on the catalyst surface and decreasing the OER onset overpotential as a result.87,88 Likewise, the catalytic activity can be influenced by the thin film resistance (R_f) by enhancing electron transfer within the bulk of the catalyst composite, leading to an increased current density. It can be observed that (Fe_{0.48}Co_{0.38}Cu_{0.14})Se showed the smallest R_f value in comparison to those of three binaries in Table 1, indicating the quaternary selenide had an enhanced conductivity and helped the local electron transfer in the catalytic system. From these studies, it is very apparent that transition metal doping improves surface electronic structure and thereby enhancing various charge transport pathways for OER catalytic activity.

The stability of any OER electrocatalyst is a critical factor to evaluate its potential in large-scale industrial application. Hence, the stability of $(Fe_{0.48}Co_{0.38}Cu_{0.14})Se$ thin film under

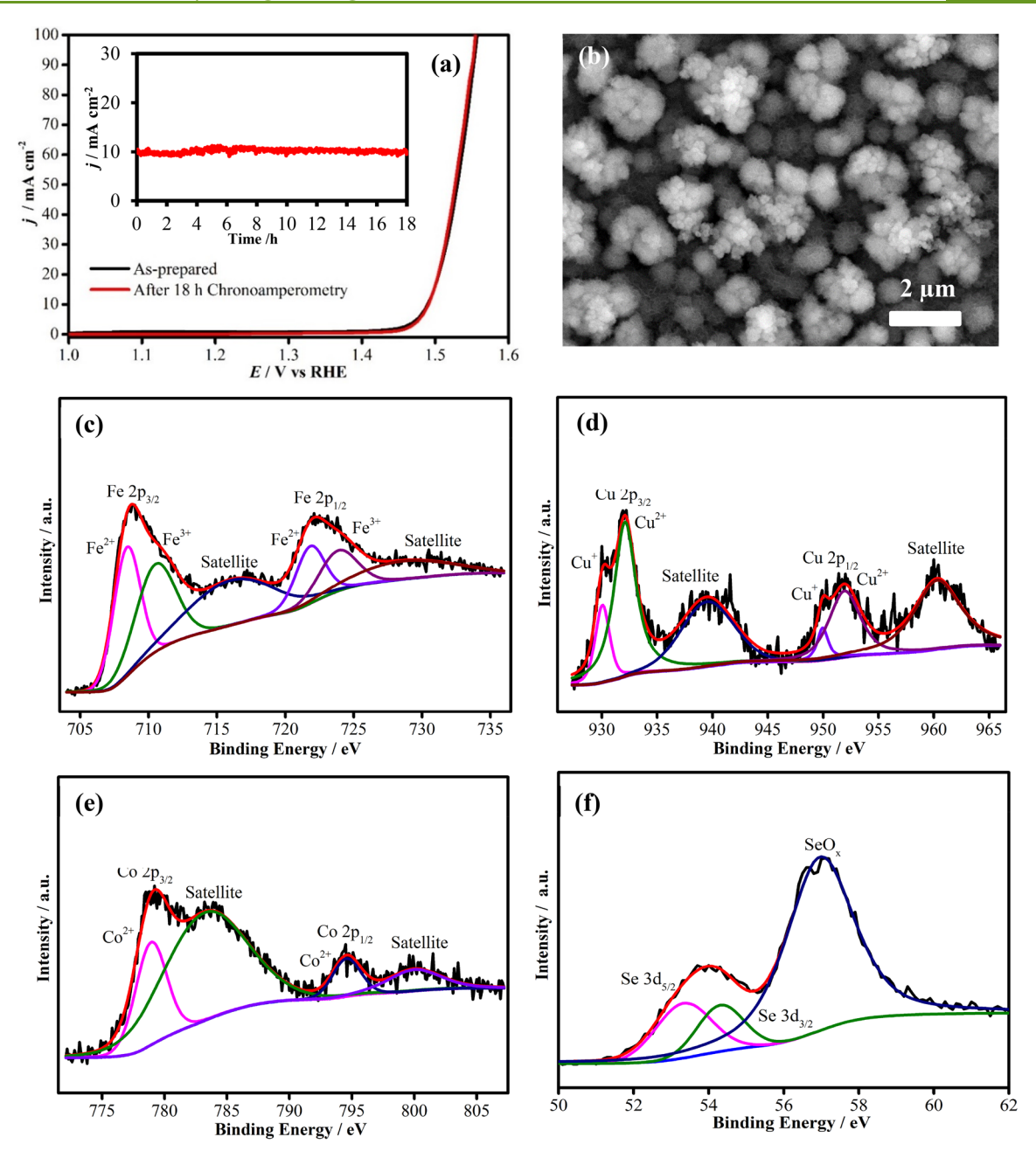


Figure 8. (a) Comparison of LSVs before and after 18 h chronoamperometry in N_2 -saturated 1.0 M KOH solution. The inset is the chronoamperometry plot of ($Fe_{0.48}Co_{0.38}Cu_{0.14}$)Se for 18 h at an applied potential of 1.50 V vs RHE. (b) SEM image of ($Fe_{0.48}Co_{0.38}Cu_{0.14}$)Se after electrochemical measurements. (c-f) XPS spectra of ($Fe_{0.48}Co_{0.38}Cu_{0.14}$)Se after chronoamperometry.

I

continuous oxygen evolution for an extended period of time (18 h) was estimated through a chronoamperometric study, as shown in the inset of Figure 8a. The chronoamperometric study was performed at a constant potential of 1.50 V vs RHE, where the thin film reached a current density of 10 mA cm $^{-2}$ in 1.0 M KOH solution. It can be observed that $(Fe_{0.48}Co_{0.38}Cu_{0.14})Se$ catalyst showed outstanding stability without any current density loss even after 18 h in the harsh alkaline medium. To confirm further the stability, the LSV of $(Fe_{0.48}Co_{0.38}Cu_{0.14})Se$ was remeasured with chronoamperometry after 18 h and was compared with that of the as-deposited catalyst shown in Figure 8a, which revealed the quaternary selenide showed almost the same catalytic activity before and after the stability study with a similar onset potential and overpotential at 10 mA cm $^{-2}$. The SEM shown in Figure 8b

exhibited that the surface morphology of (Fe_{0.48}Co_{0.38}Cu_{0.14})Se had been slightly modified by making the surface rougher possibly due to the evolution of large amounts of O₂ on catalyst surface, resulting in the production of pores. The compositional stability of the catalyst after electrochemical measurement was corroborated using XPS spectra, shown in Figure 8c–f, which revealed that the catalyst was predominantly composed of Fe, Co, Cu, and Se which were still in the mixed oxidation states. The XPS peak positions for Fe, Co, and Cu did not show any changes, indicating that the composition of the film was still selenide based. The comparison of EDS before and after chronoamperometry in Table S3 further demonstrated that the relative elemental ratio was preserved even after prolonged catalytic activity, signifying the compositional stability of the catalyst.

Interestingly, while the ternary selenides adopt various nonstoichiometric compositions including M₃Se₄, MSe, and M₃Se₂ depending on the transition metal doping, the quaternary selenides are mostly forced to adopt the monoselenide, MSe type phase. The primary difference between the M₃Se₂ and MSe structure type can be illustrated with Cu₃Se₂ and CoSe as shown in Figure S5 in the Supporting Information. In Cu₃Se₂, the transition metal is tetrahedrally coordinated to 4 Se atoms, and the CuSe₄ tetrahedra are linked further through edge sharing of the polyhedra. CoSe, on the other hand, represents the fully filled NiAs structure type containing octahedrally coordinated Co atoms, while the Se atoms show tetrahedral coordination. On doping in CoSe lattice, it can be expected that the transition metal dopant atoms will occupy the octahedral sites, while similar dopants in Cu₃Se₂ will occupy the tetrahedral sites. From the trend in catalytic activity observed here, it is apparent that for Co and Fe. the transition metal in octahedral coordination shows better catalytic activity than that in tetrahedral coordination. It has been reported previously also that Fe in the octahedral site shows better enhancement of the catalytic property. 60,64,89 Cu, on the other hand, shows better activity in tetrahedral coordination. Apart from influence of structure type and coordination geometry, other factors can also play a crucial role in determining the OER catalytic property. For example, it was reported by previous researchers that a catalyst surface containing anion vacancies and defects was favorable for the adsorption and desorption of hydroxyl species during the OER process, leading to small charge transfer resistance at the electrode-electrolyte interface and which further enhances the OER activity. 90-92 Hence, the structural defects might also play a crucial role in affecting the catalytic activity of these amorphous electrocatalysts reported in this article. However, to analyze comprehensively the role of structural defects on the OER catalytic activity, one needs to perform detailed DFT studies for each stoichiometry and related structure type. We have initiated such DFT studies and have recently observed that for one particular stoichiometry based on Cu-Co-Se, identified from this phase diagram, the structural defects on different lattice planes indeed has a significant influence on the OER catalytic activity. The results of these DFT studies will be published separately.

CONCLUSIONS

The ternary phase space of Co-Fe-Cu has been successfully explored through combinatorial electrodeposition, which has identified the optimal doping compositions that yield maximum catalytic efficiency in this family of compounds. EDS characterization of all selenide films revealed the ability of compositional control through combinatorial electrodeposition. The relative elemental compositions of the thin films were proportional to the corresponding precursor ratios in the electrolytes. A full investigation of OER kinetic parameters from sixty-six compounds revealed the trend ofcatalytic activity in Fe-Co-Cu-selenides as follows: (i) the catalytic activity is sensitive to the amount of transition metal dopants, and the presence of a relatively higher amount of Fe or Cu and a lower amount of Co leads to small overpotentials, while overpotentials tend to decrease at Fe concentration of 30-70%; (ii) quaternary selenides are more likely to show lower overpotentials as well as Tafel slopes than ternary and binary selenides, indicating the inductive effect of heteroatoms plays a crucial role in influencing the catalytic activity; (iii) Co might still be a better catalytic site, although Fe and Cu have a more positive influence on increasing catalytic activity; (iv) the enhancement in catalytic activity is supported by improved charge transfer at the catalyst—electrolyte interface and within the catalyst composite. Specifically, the best composition in this work demonstrating promising catalytic activity has been identified as (Fe_{0.48}Co_{0.38}Cu_{0.14})Se thin film with a low onset overpotential and overpotential to attain a current density of 10 mA cm $^{-2}$ of 235 and 256 mV respectively, in N₂-saturated 1.0 M KOH. This study proposes a new avenue for systematic study of mixed transition metal selenides as OER electrocatalysts employing combinatorial electrodeposition.

ASSOCIATED CONTENT

S Supporting Information

The Supporting Information is available free of charge on the ACS Publications website at DOI: 10.1021/acssuschemeng.9b01095.

Trigonal phase diagram, LSV plots, summary table, EDS table before and after chronoamperometry, atomic percentage table, and crystal structures (PDF)

AUTHOR INFORMATION

Corresponding Author

*M. Nath. Email: nathm@mst.edu.

ORCID

Manashi Nath: 0000-0002-5058-5313

Notes

The authors declare no competing financial interest.

ACKNOWLEDGMENTS

The authors acknowledge Dr. Jahangir Masud for help with some electrochemical measurements. The authors also acknowledge financial support from National Science Foundation (DMR 1710313), American Chemical Society Petroleum Research Fund (54793-ND10), and Energy Research and Development Center (ERDC) Missouri S&T. The authors also acknowledge Dr. Wenyan Liu for help with the ICP-AES measurements and Materials Research Center (MRC) for equipment usage.

REFERENCES

- (1) Chow, J.; Kopp, R. J.; Portney, P. R. Energy Resources and Global Development. *Science* **2003**, *302*, 1528–1531.
- (2) Turner, J. A. Sustainable Hydrogen Production. Science 2004, 305, 972-974.
- (3) Dresselhaus, M. S.; Thomas, I. L. Alternative Energy Technologies. *Nature* **2001**, *414*, 332–337.
- (4) Lewis, N. S. Toward Cost-Effective Solar Energy Use. Science 2007, 315, 798-801.
- (5) Walter, M. G.; Warren, E. L.; Mckone, J. R.; Boettcher, S. W.; Mi, Q.; Santori, E. A.; Lewis, N. S. Solar Water Splitting Cells. *Chem. Rev.* 2010, 110, 6446–6473.
- (6) Rossmeisl, J.; Logadottir, A.; Nørskov, J. K. Electrolysis of Water on (Oxidized) Metal Surfaces. *Chem. Phys.* **2005**, *319*, 178–184.
- (7) Suen, N.-T.; Hung, S.-F.; Quan, Q.; Zhang, N.; Xu, Y.-J.; Chen, H. M. Electrocatalysis for the Oxygen Evolution Reaction: Recent Development and Future Perspectives. *Chem. Soc. Rev.* **2017**, *46*, 337–365.
- (8) Dau, H.; Limberg, C.; Reier, T.; Risch, M.; Roggan, S.; Strasser, P. The Mechanism of Water Oxidation: From Electrolysis via Homogeneous to Biological Catalysis. *ChemCatChem* **2010**, *2*, 724–761.

- (9) Yan, Y.; Xia, B. Y.; Zhao, B.; Wang, X. A Review on Noble-Metal-Free Bifunctional Heterogeneous Catalysts for Overall Electrochemical Water Splitting. *J. Mater. Chem. A* **2016**, *4*, 17587–17603.
- (10) Görlin, Y.; Jaramillo, T. F. A Bifunctional Nonprecious Metal Catalyst for Oxygen Reduction and Water Oxidation. *J. Am. Chem. Soc.* **2010**, *132*, 13612–13614.
- (11) Chen, Q.; Switzer, J. A. Photoelectrochemistry of Ultrathin, Semitransparent, and Catalytic Gold Films Electrodeposited Epitaxially onto n-Silicon (111). ACS Appl. Mater. Interfaces 2018, 10, 21365–21371.
- (12) Mahenderkar, N. K.; Chen, Q.; Liu, Y. C.; Duchild, A. R.; Hofheins, S.; Chason, E.; Switzer, J. A. Epitaxial Lift-off of Electrodeposited Single-Crystal Gold Foils for Flexible Electronics. *Science* **2017**, 355, 1203–1206.
- (13) Wang, H.; Lee, H.; Deng, Y.; Lu, Z.; Hsu, P.; Liu, Y.; Lin, D.; Cui, Y. Bifunctional Non-Noble Metal Oxide Nanoparticle Electrocatalysts through Lithium-Induced Conversion for Overall Water Splitting. *Nat. Commun.* **2015**, *6*, 7261.
- (14) Suntivich, J.; May, K. J.; Gasteiger, H. A.; Goodenough, J. B.; Shao-Horn, Y. A Perovskite Oxide Optimized for Oxygen Evolution Catalysis from Molecular Orbital Principles. *Science* **2011**, 334, 1383–1385.
- (15) Over, H. Surface Chemistry of Ruthenium Dioxide in Heterogeneous Catalysis and Electrocatalysis: From Fundamental to Applied Research. *Chem. Rev.* **2012**, *112*, 3356–3426.
- (16) Reier, T.; Teschner, D.; Lunkenbein, T.; Bergmann, A.; Selve, S.; Kraehnert, R.; Schlogl, R.; Strasser, P. Electrocatalytic Oxygen Evolution on Iridium Oxide: Uncovering Catalyst-Substrate Interactions and Active Iridium Oxide Species. *J. Electrochem. Soc.* **2014**, *161*, F876—F882.
- (17) McCrory, C. C. L.; Jung, S.; Peters, J. C.; Jaramillo, T. F. Benchmarking Heterogeneous Electrocatalysts for the Oxygen Evolution Reaction. *J. Am. Chem. Soc.* **2013**, *135*, 16977–16987.
- (18) Gao, X.; Zhang, H.; Li, Q.; Yu, X.; Hong, Z.; Zhang, X.; Liang, C.; Lin, Z. Hierarchical NiCo₂O₄ Hollow Microcuboids as Bifunctional Electrocatalysts for Overall Water-Splitting. *Angew. Chem., Int. Ed.* **2016**, *55*, 6290–6294.
- (19) Görlin, M.; Chernev, P.; Ferreira de Araújo, J.; Reier, T.; Dresp, S.; Paul, B.; Krähnert, R.; Dau, H.; Strasser, P. Oxygen Evolution Reaction Dynamics, Faradaic Charge Efficiency, and the Active Metal Redox States of Ni-Fe Oxide Water Splitting Electrocatalysts. *J. Am. Chem. Soc.* **2016**, 138, 5603–5614.
- (20) Chen, Q.; Switzer, J. A. Electrodeposition of Nanometer-Thick Epitaxial Films of Silver onto Single-Crystal Silicon Wafers. *J. Mater. Chem. C* **2019**, *7*, 1720–1725.
- (21) Gong, M.; Li, Y.; Wang, H.; Liang, Y.; Wu, J. Z.; Zhou, J.; Wang, J.; Regier, T.; Wei, F.; Dai, H. An Advanced Ni-Fe Layered Double Hydroxide Electrocatalyst for Water Oxidation. *J. Am. Chem. Soc.* 2013, 135, 8452–8455.
- (22) Kuang, M.; Han, P.; Wang, Q.; Li, J.; Zheng, G. CuCo Hybrid Oxides as Bifunctional Electrocatalyst for Efficient Water Splitting. *Adv. Funct. Mater.* **2016**, *26*, 8555–8561.
- (23) Chemelewski, W. D.; Lee, H. C.; Lin, J. F.; Bard, A. J.; Mullins, C. B. Amorphous FeOOH Oxygen Evolution Reaction Catalyst for Photoelectrochemical Water Splitting. *J. Am. Chem. Soc.* **2014**, *136*, 2843–2850.
- (24) Deng, X.; Tüysüz, H. Cobalt-Oxide-Based Materials as Water Oxidation Catalyst: Recent Progress and Challenges. *ACS Catal.* **2014**, *4*, 3701–3714.
- (25) Anantharaj, S.; Ede, S. R.; Sakthikumar, K.; Karthick, K.; Mishra, S.; Kundu, S. Recent Trends and Perspectives in Electrochemical Water Splitting with an Emphasis on Sulfide, Selenide, and Phosphide Catalysts of Fe, Co, and Ni: A Review. ACS Catal. 2016, 6, 8069–8097.
- (26) Swesi, A. T.; Masud, J.; Nath, M. Nickel Selenide as a High-Efficiency Catalyst for Oxygen Evolution Reaction. *Energy Environ. Sci.* **2016**, *9*, 1771–1782.
- (27) Tang, C.; Cheng, N.; Pu, Z.; Xing, W.; Sun, X. NiSe Nanowire Film Supported on Nickel Foam: An Efficient and Stable 3D

- Bifunctional Electrode for Full Water Splitting. Angew. Chem., Int. Ed. 2015, 54, 9351–9355.
- (28) Kwak, I. H.; Im, H. S.; Jang, D. M.; Kim, Y. W.; Park, K.; Lim, Y. R.; Cha, E. H.; Park, J. CoSe₂ and NiSe₂ Nanocrystals as Superior Bifunctional Catalysts for Electrochemical and Photoelectrochemical Water Splitting. *ACS Appl. Mater. Interfaces* **2016**, *8*, 5327–5334.
- (29) Li, W.; Gao, X.; Xiong, D.; Wei, F.; Song, W. G.; Xu, J.; Liu, L. Hydrothermal Synthesis of Monolithic Co₃Se₄ Nanowire Electrodes for Oxygen Evolution and Overall Water Splitting with High Efficiency and Extraordinary Catalytic Stability. *Adv. Energy Mater.* **2017**, *7*, 1602579.
- (30) De Silva, U.; Masud, J.; Zhang, N.; Hong, Y.; Liyanage, W. P. R.; Asle Zaeem, M.; Nath, M. Nickel Telluride as a Bifunctional Electrocatalyst for Efficient Water Splitting in Alkaline Medium. *J. Mater. Chem. A* **2018**, *6*, 7608–7622.
- (31) Xu, K.; Ding, H.; Lv, H.; Tao, S.; Chen, P.; Wu, X.; Chu, W.; Wu, C.; Xie, Y. Understanding Structure-Dependent Catalytic Performance of Nickel Selenides for Electrochemical Water Oxidation. ACS Catal. 2017, 7, 310–315.
- (32) Carlson, R. R.; Meek, D. W. Dipole Moments of Several Tertiary Phosphine Oxides, Sulfides, and Selenides and of Some Tertiary Arsine Oxides and Sulfides. *Inorg. Chem.* **1974**, *13*, 1741–1747.
- (33) Cao, X.; Hong, Y.; Zhang, N.; Chen, Q.; Masud, J.; Zaeem, M. A.; Nath, M. Phase Exploration and Identification of Multinary Transition-Metal Selenides as High-Efficiency Oxygen Evolution Electrocatalysts through Combinatorial Electrodeposition. *ACS Catal.* **2018**, *8*, 8273–8289.
- (34) Swesi, A. T.; Masud, J.; Liyanage, W. P. R.; Umapathi, S.; Bohannan, E.; Medvedeva, J.; Nath, M. Textured NiSe₂ Film: Bifunctional Electrocatalyst for Full Water Splitting at Remarkably Low Overpotential with High Energy Efficiency. Sci. Rep. 2017, 7, 2401.
- (35) Gao, M. R.; Cao, X.; Gao, Q.; Xu, Y. F.; Zheng, Y. R.; Jiang, J.; Yu, S. H. Nitrogen-Doped Graphene Supported CoSe₂ Nanobelt Composite Catalyst for Efficient Water Oxidation. *ACS Nano* **2014**, *8*, 3970–3978.
- (36) Masud, J.; Swesi, A. T.; Liyanage, W. P. R.; Nath, M. Cobalt Selenide Nanostructures: An Efficient Bifunctional Catalyst with High Current Density at Low Coverage. *ACS Appl. Mater. Interfaces* **2016**, 8, 17292–17302.
- (37) Liu, B.; Zhao, Y. F.; Peng, H. Q.; Zhang, Z. Y.; Sit, C. K.; Yuen, M. F.; Zhang, T. R.; Lee, C. S.; Zhang, W. J. Nickel-Cobalt Diselenide 3D Mesoporous Nanosheet Networks Supported on Ni Foam: An All-pH Highly Efficient Integrated Electrocatalyst for Hydrogen Evolution. *Adv. Mater.* **2017**, *29*, 1606521.
- (38) Xu, X.; Song, F.; Hu, X. A Nickel Iron Diselenide-Derived Efficient Oxygen-Evolution Catalyst. *Nat. Commun.* **2016**, *7*, 12324.
- (39) Umapathi, S.; Masud, J.; Swesi, A. T.; Nath, M. FeNi₂Se₄-Reduced Graphene Oxide Nanocomposite: Enhancing Bifunctional Electrocatalytic Activity for Oxygen Evolution and Reduction through Synergistic Effects. *Adv. Sustainable Syst.* **2017**, *1*, 1700086.
- (40) Akbar, K.; Jeon, J. H.; Kim, M.; Jeong, J.; Yi, Y.; Chun, S.-H. Bifunctional Electrodeposited 3D NiCoSe₂/Nickle Foam Electrocatalysts for Its Applications in Enhanced Oxygen Evolution Reaction and for Hydrazine Oxidation. *ACS Sustainable Chem. Eng.* **2018**, *6*, 7735–7742.
- (41) Suen, N. T.; Hung, S. F.; Quan, Q.; Zhang, N.; Xu, Y. J.; Chen, H. M. Electrocatalysis for the Oxygen Evolution Reaction: Recent Development and Future Perspectives. *Chem. Soc. Rev.* **2017**, *46*, 337–365.
- (42) Maiyalagan, T.; Jarvis, K. A.; Therese, S.; Ferreira, P. J.; Manthiram, A. Spinel-Type Lithium Cobalt Oxide as a Bifunctional Electrocatalyst for the Oxygen Evolution and Oxygen Reduction Reactions. *Nat. Commun.* **2014**, *5*, 3949.
- (43) Gong, M.; Dai, H. A Mini Review on NiFe-Based Materials as Highly Active Oxygen Evolution Reaction Electrocatalysts. *Nano Res.* **2015**, *8*, 23–39.

- (44) Enman, L. J.; Burke, M. S.; Batchellor, A. S.; Boettcher, S. W. Effects of Intentionally Incorporated Metal Cations on the Oxygen Evolution Electrocatalytic Activity of Nickel (Oxy) Hydroxide in Alkaline Media. *ACS Catal.* **2016**, *6*, 2416–2423.
- (45) Görlin, M.; Ferreira de Araujo, J.; Schmies, H.; Bernsmeier, D.; Dresp, S.; Gliech, M.; Jusys, Z.; Chernev, P.; Kraehnert, R.; Dau, H.; Strasser, P. Tracking Catalyst Redox States and Reaction Dynamics in Ni-Fe Oxyhydroxide Oxygen Evolution Reaction Electrocatalysts: The Role of Catalyst Support and Electrolyte PH. *J. Am. Chem. Soc.* 2017, 139, 2070–2082.
- (46) Yang, Y.; Fei, H.; Ruan, G.; Xiang, C.; Tour, J. M. Efficient Electrocatalytic Oxygen Evolution on Amorphous Nickel-Cobalt Binary Oxide Nanoporous Layers. *ACS Nano* **2014**, *8*, 9518–9523.
- (47) Simon, G.; Kesler, S. E.; Essene, E. J. Phase Relations among Selenides, Sulfides, Tellurides, and Oxides: II. Applications to Selenide-Bearing Ore Deposits. *Econ. Geol. Bull. Soc. Econ. Geol.* 1997, 92, 468–484.
- (48) Xu, H.; Feng, J. X.; Tong, Y. X.; Li, G. R. Cu₂O-Cu Hybrid Foams as High-Performance Electrocatalysts for Oxygen Evolution Reaction in Alkaline Media. *ACS Catal.* **2017**, *7*, 986–991.
- (49) Zhang, H.; Zhang, Z.; Li, N.; Yan, W.; Zhu, Z. Cu₂O@C Core/ Shell Nanoparticle as an Electrocatalyst for Oxygen Evolution Reaction. J. Catal. 2017, 352, 239–245.
- (50) Masud, J.; Liyanage, W. P. R.; Cao, X.; Saxena, A.; Nath, M. Copper Selenides as High-Efficiency Electrocatalysts for Oxygen Evolution Reaction. *ACS Appl. Energy Mater.* **2018**, *1*, 4075–4083.
- (51) Cao, X.; Johnson, E.; Nath, M. Identifying High-efficiency Oxygen Evolution Electrocatalysts from Co-Ni-Cu Based Selenides through Combinatorial Electrodeposition. *J. Mater. Chem. A* **2019**, 7, 9877–9889.
- (52) Batchellor, A. S.; Kwon, G.; Laskowski, F. A. L.; Tiede, D. M.; Boettcher, S. W. Domain Structures of Ni and NiFe (Oxy)Hydroxide Oxygen-Evolution Catalysts from X-Ray Pair Distribution Function Analysis. *J. Phys. Chem. C* **2017**, *121*, 25421–25429.
- (53) Zhuang, L.; Ge, L.; Yang, Y.; Li, M.; Jia, Y.; Yao, X.; Zhu, Z. Ultrathin Iron-Cobalt Oxide Nanosheets with Abundant Oxygen Vacancies for the Oxygen Evolution Reaction. *Adv. Mater.* **2017**, 29, 1606793.
- (54) Santos, E.; Schmickler, W. d-Band Catalysis in Electrochemistry. *ChemPhysChem* **2006**, 7, 2282–2285.
- (55) Stevens, M. B.; Trang, C. D. M.; Enman, L. J.; Deng, J.; Boettcher, S. W. Reactive Fe-Sites in Ni/Fe (Oxy)Hydroxide Are Responsible for Exceptional Oxygen Electrocatalysis Activity. *J. Am. Chem. Soc.* **2017**, *139*, 11361–11364.
- (56) Xu, D.; Stevens, M. B.; Rui, Y.; DeLuca, G.; Boettcher, S. W.; Reichmanis, E.; Li, Y.; Zhang, Q.; Wang, H. The Role of Cr Doping in Ni-Fe Oxide/(Oxy)Hydroxide Electrocatalysts for Oxygen Evolution. *Electrochim. Acta* **2018**, 265, 10–18.
- (57) Burke, M. S.; Kast, M. G.; Trotochaud, L.; Smith, A. M.; Boettcher, S. W. Cobalt-Iron (Oxy)Hydroxide Oxygen Evolution Electrocatalysts: The Role of Structure and Composition on Activity, Stability, and Mechanism. *J. Am. Chem. Soc.* **2015**, *137*, 3638–3648.
- (58) Xu, X.; Liang, H.; Ming, F.; Qi, Z.; Xie, Y.; Wang, Z. Prussian Blue Analogues Derived Penroseite (Ni, Co)Se₂ Nanocages Anchored on 3D Graphene Aerogel for Efficient Water Splitting. *ACS Catal.* **2017**, *7*, 6394–6399.
- (59) Zhao, X.; Zhang, H.; Yan, Y.; Cao, J.; Li, X.; Zhou, S.; Peng, Z.; Zeng, J. Engineering the Electrical Conductivity of Lamellar Silver-Doped Cobalt (II) Selenide Nanobelts for Enhanced Oxygen Evolution. *Angew. Chem., Int. Ed.* **2017**, *56*, 328–332.
- (60) Trotochaud, L.; Young, S. L.; Ranney, J. K.; Boettcher, S. W. Nickel-Iron Oxyhydroxide Oxygen-Evolution Electrocatalysts: The Role of Intentional and Incidental Iron Incorporation. *J. Am. Chem. Soc.* **2014**, *136*, 6744–6753.
- (61) Qi, J.; Zhang, W.; Xiang, R.; Liu, K.; Wang, H. Y.; Chen, M.; Han, Y.; Cao, R. Porous Nickel-Iron Oxide as a Highly Efficient Electrocatalyst for Oxygen Evolution Reaction. *Adv. Sci.* **2015**, *2*, 1500199.

- (62) Wang, Z.; Li, J.; Tian, X.; Wang, X.; Yu, Y.; Owusu, K. A.; He, L.; Mai, L. Porous Nickel-Iron Selenide Nanosheets as Highly Efficient Electrocatalysts for Oxygen Evolution Reaction. *ACS Appl. Mater. Interfaces* **2016**, *8*, 19386–19392.
- (63) Li, Y. F.; Selloni, A. Mechanism and Activity of Water Oxidation on Selected Surfaces of Pure and Fe-Doped NiO_x. ACS Catal. **2014**, *4*, 1148–1153.
- (64) Landon, J.; Demeter, E.; Inoğlu, N.; Keturakis, C.; Wachs, I. E.; Vasić, R.; Frenkel, A. I.; Kitchin, J. R. Spectroscopic Characterization of Mixed Fe-Ni Oxide Electrocatalysts for the Oxygen Evolution Reaction in Alkaline Electrolytes. *ACS Catal.* **2012**, *2*, 1793–1801.
- (65) Enman, L. J.; Stevens, M. B.; Dahan, M. H.; Nellist, M. R.; Toroker, M. C.; Boettcher, S. W. Operando X-Ray Absorption Spectroscopy Shows Iron Oxidation Is Concurrent with Oxygen Evolution in Cobalt-Iron (Oxy)Hydroxide Electrocatalysts. *Angew. Chem., Int. Ed.* **2018**, *57*, 12840–12844.
- (66) Zhang, X.; Zhang, X.; Xu, H.; Wu, Z.; Wang, H.; Liang, Y. Iron-Doped Cobalt Monophosphide Nanosheet/Carbon Nanotube Hybrids as Active and Stable Electrocatalysts for Water Splitting. *Adv. Funct. Mater.* **2017**, 27, 1606635.
- (67) Zhang, J.; Wang, Y.; Zhang, C.; Gao, H.; Lv, L.; Han, L.; Zhang, Z. Self-Supported Porous NiSe₂ Nanowrinkles as Efficient Bifunctional Electrocatalysts for Overall Water Splitting. *ACS Sustainable Chem. Eng.* **2018**, *6*, 2231–2239.
- (68) Anantharaj, S.; Kennedy, J.; Kundu, S. Microwave-Initiated Facile Formation of Ni₃Se₄ Nanoassemblies for Enhanced and Stable Water Splitting in Neutral and Alkaline Media. *ACS Appl. Mater. Interfaces* **2017**, *9*, 8714–8728.
- (69) Friebel, D.; Louie, M. W.; Bajdich, M.; Sanwald, K. E.; Cai, Y.; Wise, A. M.; Cheng, M. J.; Sokaras, D.; Weng, T. C.; Alonso-Mori, R.; Davis, R. C.; Bargar, J. R.; Nørskov, J. K.; Nilsson, A.; Bell, A. T. Identification of Highly Active Fe Sites in (Ni, Fe)OOH for Electrocatalytic Water Splitting. *J. Am. Chem. Soc.* **2015**, *137*, 1305–1313.
- (70) Shinagawa, T.; Garcia-Esparza, A. T.; Takanabe, K. Insight on Tafel Slopes from a Microkinetic Analysis of Aqueous Electrocatalysis for Energy Conversion. *Sci. Rep.* **2015**, *5*, 13801.
- (71) Chi, J. Q.; Yan, K. L.; Xiao, Z.; Dong, B.; Shang, X.; Gao, W. K.; Li, X.; Chai, Y. M.; Liu, C. G. Trimetallic Ni-Fe-Co Selenides Nanoparticles Supported on Carbon Fiber Cloth as Efficient Electrocatalyst for Oxygen Evolution Reaction. *Int. J. Hydrogen Energy* **2017**, *42*, 20599–20607.
- (72) Smith, R. D. L.; Prévot, M. S.; Fagan, R. D.; Trudel, S.; Berlinguette, C. P. Water Oxidation Catalysis: Electrocatalytic Response to Metal Stoichiometry in Amorphous Metal Oxide Films Containing Iron, Cobalt, and Nickel. J. Am. Chem. Soc. 2013, 135, 11580–11586.
- (73) Grimaud, A.; May, K. J.; Carlton, C. E.; Lee, Y. L.; Risch, M.; Hong, W. T.; Zhou, J.; Shao-Horn, Y. Double Perovskites as a Family of Highly Active Catalysts for Oxygen Evolution in Alkaline Solution. *Nat. Commun.* **2013**, *4*, 2439.
- (74) Shen, M.; Ruan, C.; Chen, Y.; Jiang, C.; Ai, K.; Lu, L. Covalent Entrapment of Cobalt-Iron Sulfides in N-Doped Mesoporous Carbon: Extraordinary Bifunctional Electrocatalysts for Oxygen Reduction and Evolution Reactions. *ACS Appl. Mater. Interfaces* **2015**, *7*, 1207–1218.
- (75) Zhang, P.; Li, L.; Nordlund, D.; Chen, H.; Fan, L.; Zhang, B.; Sheng, X.; Daniel, Q.; Sun, L. Dendritic Core-Shell Nickel-Iron-Copper Metal/Metal Oxide Electrode for Efficient Electrocatalytic Water Oxidation. *Nat. Commun.* **2018**, *9*, 381.
- (76) Liu, Y.; Niu, Z.; Lu, Y.; Zhang, L.; Yan, K. Facile Synthesis of CuFe₂O₄ crystals Efficient for Water Oxidation and H₂O₂ reduction. *J. Alloys Compd.* **2018**, 735, 654–659.
- (77) Chen, H.; Gao, Y.; Ye, L.; Yao, Y.; Chen, X.; Wei, Y.; Sun, L. A Cu₂Se-Cu₂O Film Electrodeposited on Titanium Foil as a Highly Active and Stable Electrocatalyst for the Oxygen Evolution Reaction. *Chem. Commun.* **2018**, *54*, 4979–4982.
- (78) Niu, Y.; Qian, X.; Xu, C.; Liu, H.; Wu, W.; Hou, L. Cu-Ni-CoSe, Quaternary Porous Nanocubes as Enhanced Pt-Free Electro-

- catalysts for Highly Efficient Dye-Sensitized Solar Cells and Hydrogen Evolution in Alkaline Medium. *Chem. Eng. J.* **2019**, *357*, 11–20.
- (79) Ali, Z.; Asif, M.; Huang, X.; Tang, T.; Hou, Y. Hierarchically Porous Fe₂CoSe₄ Binary-Metal Selenide for Extraordinary Rate Performance and Durable Anode of Sodium-Ion Batteries. *Adv. Mater.* **2018**, *30*, 1802745.
- (80) Zhao, Y.; Jin, B.; Zheng, Y.; Jin, H.; Jiao, Y.; Qiao, S. Z. Charge State Manipulation of Cobalt Selenide Catalyst for Overall Seawater Electrolysis. *Adv. Energy Mater.* **2018**, *8*, 1801926.
- (81) Yu, J.; Cheng, G.; Luo, W. 3D Mesoporous Rose-like Nickel-Iron Selenide Microspheres as Advanced Electrocatalysts for the Oxygen Evolution Reaction. *Nano Res.* **2018**, *11*, 2149–2158.
- (82) Quan, L.; Liu, T.; Yi, M.; Chen, Q.; Cai, D.; Zhan, H. Construction of Hierarchical Nickel Cobalt Selenide Complex Hollow Spheres for Pseudocapacitors with Enhanced Performance. *Electro-chim. Acta* **2018**, 281, 109–116.
- (83) Jia, J.; Seitz, L. C.; Benck, J. D.; Huo, Y.; Chen, Y.; Ng, J. W. D.; Bilir, T.; Harris, J. S.; Jaramillo, T. F. Solar Water Splitting by Photovoltaic-Electrolysis with a Solar-to-Hydrogen Efficiency over 30%. *Nat. Commun.* **2016**, *7*, 13237.
- (84) Xiao, P.; Sk, M. A.; Thia, L.; Ge, X.; Lim, R. J.; Wang, J. Y.; Lim, K. H.; Wang, X. Molybdenum Phosphide as an Efficient Electrocatalyst for the Hydrogen Evolution Reaction. *Energy Environ. Sci.* **2014**, *7*, 2624–2629.
- (85) Merki, D.; Vrubel, H.; Rovelli, L.; Fierro, S.; Hu, X. Fe, Co, and Ni Ions Promote the Catalytic Activity of Amorphous Molybdenum Sulfide Films for Hydrogen Evolution. *Chem. Sci.* **2012**, *3*, 2515–2525.
- (86) Sivanantham, A.; Ganesan, P.; Shanmugam, S. Hierarchical NiCo₂S₄ Nanowire Arrays Supported on Ni Foam: An Efficient and Durable Bifunctional Electrocatalyst for Oxygen and Hydrogen Evolution Reactions. *Adv. Funct. Mater.* **2016**, 26, 4661–4672.
- (87) Chen, P.; Xu, K.; Zhou, T.; Tong, Y.; Wu, J.; Cheng, H.; Lu, X.; Ding, H.; Wu, C.; Xie, Y. Strong-Coupled Cobalt Borate Nanosheets/Graphene Hybrid as Electrocatalyst for Water Oxidation under Both Alkaline and Neutral Conditions. *Angew. Chem., Int. Ed.* **2016**, *55*, 2488–2492.
- (88) Jia, X.; Zhao, Y.; Chen, G.; Shang, L.; Shi, R.; Kang, X.; Waterhouse, G. I. N.; Wu, L. Z.; Tung, C. H.; Zhang, T. Ni₃FeN Nanoparticles Derived from Ultrathin NiFe-Layered Double Hydroxide Nanosheets: An Efficient Overall Water Splitting Electrocatalyst. *Adv. Energy Mater.* **2016**, *6*, 1502585.
- (89) Schwanke, C.; Stein, H. S.; Xi, L.; Sliozberg, K.; Schuhmann, W.; Ludwig, A.; Lange, K. M. Correlating Oxygen Evolution Catalysts Activity and Electronic Structure by a High-Throughput Investigation of Ni_{1-y-z}Fe_yCr_zO_x. Sci. Rep. **2017**, *7*, 44192.
- (90) Yan, X.; Tian, L.; Li, K.; Atkins, S.; Zhao, H.; Murowchick, J.; Liu, L.; Chen, X. FeNi₃/NiFeO_x Nanohybrids as Highly Efficient Bifunctional Electrocatalysts for Overall Water Splitting. *Adv. Mater. Interfaces* **2016**, *3*, 1600368.
- (91) Yan, X.; Tian, L.; Atkins, S.; Liu, Y.; Murowchick, J.; Chen, X. Converting CoMoO₄ into CoO/MoO_x for Overall Water Splitting by Hydrogenation. *ACS Sustainable Chem. Eng.* **2016**, *4*, 3743–3749.
- (92) Liu, L.; Niu, D.; Song, F.; Lyu, L.; He, J.; Yan, X.; Li, K.; Hu, X.; Chen, X. From Water Oxidation to Reduction: Transformation from Ni_xCo_{3-x}O₄ Nanowires to NiCo/NiCoO_x Heterostructures. *ACS Appl. Mater. Interfaces* **2016**, *8*, 3208–3214.